J. Fluid Mech. (2009), *vol.* 628, *pp.* 427–443. © 2009 Cambridge University Press
doi:10.1017/S0022112009006715 Printed in the United Kingdom

A similarity solution for a dual moving boundary problem associated with a coastal-plain depositional system

JORGE LORENZO-TRUEBA[1], VAUGHAN R. VOLLER[1]†, TETSUJI MUTO[2], WONSUCK KIM[3], CHRIS PAOLA[4] AND JOHN B. SWENSON[5]

[1]St. Anthony Falls Laboratory, Department of Civil Engineering, University of Minnesota, Minneapolis, MN 55414, USA

[2]Faculty of Environmental Studies, Nagasaki University, Nagasaki, Japan

[3]Department of Geological Sciences, Jackson School of Geosciences, University of Texas, Austin, TX 78712, USA

[4]St. Anthony Falls Laboratory, Department of Geology and Geophysics, University of Minnesota, Minneapolis, MN 55414, USA

[5]Department of Geological Sciences, University of Minnesota, Duluth, MN 55812, USA

(Received 22 August 2008 and in revised form 20 February 2009)

Assuming that the sediment flux in the Exner equation can be linearly related to the local bed slope, we establish a one-dimensional model for the bed-load transport of sediment in a coastal-plain depositional system, such as a delta and a continental margin. The domain of this model is defined by two moving boundaries: the shoreline and the alluvial–bedrock transition. These boundaries represent fundamental transitions in surface morphology and sediment transport regime, and their trajectories in time and space define the evolution of the shape of the sedimentary prism. Under the assumptions of fixed bedrock slope and sea level the model admits a closed-form similarity solution for the movements of these boundaries. A mapping of the solution space, relevant to field scales, shows two domains controlled by the relative slopes of the bedrock and fluvial surface: one in which changes in environmental parameters are mainly recorded in the upstream boundary and another in which these changes are mainly recorded in the shoreline. We also find good agreement between the analytical solution and laboratory flume experiments for the movements of the alluvial–bedrock transition and the shoreline.

1. Introduction

Coastal areas such as deltas and continental margins are composites of several primary sedimentary environments: at a minimum, a depositional fluvial region and an offshore region (figure 1). The latter may include sub-regions (e.g. wave-dominated shelf, mass-flow-dominated slope). The depositional fluvial region typically terminates upstream in a transition to a bedrock fluvial region. The boundaries between these regions, which are often readily visible on topographic maps, represent fundamental qualitative transitions in the processes by which sediment is transported. In fact the

† Email address for correspondence: volle001@umn.edu

https://doi.org/10.1017/S0022112009006715 Published online by Cambridge University Press

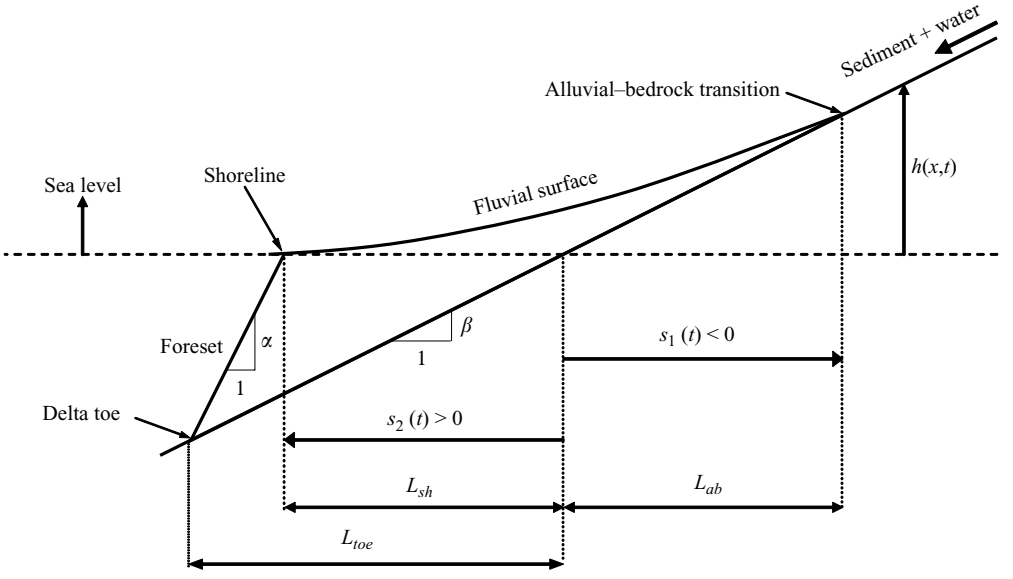


FIGURE 1. Schematic of sediment basin problem. (Note the seaward direction is assigned positive.)

shape, large-scale structure and long-term evolution of coastal sedimentary systems are the result of the complex interplay of the different transport regions, and the boundaries separating them are moving boundaries – internal boundaries whose location must be determined as part of the solution to the overall morphological evolution problem (Marr *et al.* 2000; Swenson *et al.* 2000; Voller, Swenson & Paola 2004; Kim & Muto 2007; Swenson & Muto 2007). The classical moving boundary problem involves the tracking of the solid–liquid interface during the melting of ice and is known as the Stefan problem (Crank 1984). The first application of moving boundary models to morphodynamics was by Swenson *et al.* (2000). These authors used an analogy between heat and sediment diffusive transport to develop a generalized Stefan-like model to describe the movement on planetary time scales of the shoreline in a sedimentary continental margin under varying conditions of sediment influx, sea level and tectonic subsidence. In the limit of constant bedrock slope (no subsidence) and sea level, Voller *et al.* (2004) developed a closed-form similarity solution for the Swenson model which tracks the shoreline movement in a one-dimensional domain driven by a prescribed sediment flux. This solution has common elements with the classic Neumann similarity solution of the Stefan one-phase melting problem (Crank 1984). The key differences in the model presented in Voller *et al.* (2004) from the classic solution are (i) a specified flux at the origin $x = 0$ and (ii) a spatially variable latent heat (ocean depth). The ideas in Voller *et al.* (2004) have recently been used by Capart, Bellal & Young (2007) and Lai & Capart (2007) to develop analytical solutions for a more extensive solution domain, extending from the alluvial–bedrock transition (the upstream end of a sediment prism developed over the non-erodible bedrock basement) located at $x = s_1(t) < 0$ through to the shoreline (the sediment–water interface) located at $x = s_2(t) > 0$. These authors essentially developed two similarity solutions; one solves for the movement of the alluvial–bedrock transition, s_1, in the upstream direction when the downstream condition is set at $s_2 \to \infty$; the other solves for the downstream (progradation) of the

https://doi.org/10.1017/S0022112009006715 Published online by Cambridge University Press

shoreline, s_2, when the upstream condition is set at $s_1 \to \infty$. There is, however, no need to look at the limit settings of the upstream and downstream boundary conditions. It is generally accepted that the geometry of modern river deltas resembles a triangular prism in longitudinal section, superimposed upon a relatively flat basement profile (Posamentier *et al.* 1992). These domain transitions of the coastal prism are typically marked by changes in surface slope and/or grain size. A general treatment for this problem is to construct a transient model with the initial setting of $s_1 = s_2 = 0$ and allow for the subsequent downstream movement of the shoreline in the positive x-direction and the upstream movement of the alluvial–bedrock transition in the negative x-direction. As noted by Parker & Muto (2003), an interesting feature of this case is that it simultaneously admits two moving boundaries: the shoreline and alluvial–bedrock transition. This feature is found in other systems, notably the liquidus and eutectic fronts in the solidification of binary eutectic alloys (Worster 1986; Voller 1997). In terms of the sediment problem, Parker & Muto (2003) developed a basic numerical scheme to track the evolution of the moving boundaries. In recent attempts to track these boundaries Swenson & Muto (2007) presented a refined numerical treatment based on a Landau front-fixing approach (Crank 1984), and Kim & Muto (2007) employed a geometric mass balance model. To date, however, no closed analytical solution of the two moving boundaries model based on the diffusive transport model in Swenson *et al.* (2000) has been presented in the literature. The objective of this paper is to develop such a solution, examine its implications for response of coastal prisms to imposed changes and compare the solutions with measurements from flume experiments.

2. Governing equations

In the problem at hand, we identify two regions, a sub-aerial fluvial region upstream of the shoreline and a submarine offshore region. As noted above, the depositional fluvial region, which can be referred to as a fluvial plain, is bounded upstream by an alluvial–bedrock transition and downstream by the shoreline. Typically this plain can extend over 10 km or even 100 km. At a given instant of time the shoreline boundary may be quite irregular; e.g. at channel and river mouths, deltas will grow radially ahead of the surrounding shoreline. On large time scales, however, due to avulsion (repositioning of channels) events such features can be averaged out. Hence it is reasonable, to first order, to represent the evolution of the system by the one-dimensional longitudinal section shown in figure 1.

The mechanism of transport of sediment in each of the domains in figure 1 is significantly different. In the sub-aerial fluvial region the sediment is transported through the channel system primarily as bed load; i.e. sediment particles move in a layer along the channel beds via modes such as shear-stress-induced saltation. The downstream decrease in slope in this region results in a reduction in the bed shear stress, leading to a deposition of sediment in the channel. On non-channelized portions of the fluvial region sediment is deposited by flood events and at larger time scales by channel avulsion. In contrast, in the offshore region sediment transport primarily occurs by slope failure (avalanching) – which may induce gravity currents – in addition to transport as suspended load driven by wind, wave and tide forces (Sommerfield *et al.* 2007).

Using figure 1 as a reference, a suitable governing sediment transport equation is derived by considering the deposition of a sediment prism on to a non-erodible bedrock surface set at constant slope β. At time $t = 0$, with no sediment deposited,

https://doi.org/10.1017/S0022112009006715 Published online by Cambridge University Press

the sea level intersects the bedrock surface at $x = 0$. To retain some generality we initially assume that the bedrock surface undergoes a uniform subsidence or uplift – i.e. there is no spatial variation in subsidence/uplift rate. In this way, geometric changes in the domain are defined by the rise or fall of sea level relative to the background subsidence/uplift. At times $t > 0$, the sediment prism starts to grow at $x = 0$ by a steady sediment unit flux $\overline{q}_0$ (volumetric sediment bed transport per unit width and time) introduced at the far field upstream boundary and bypassed over the bedrock basement to the sediment prism. Note the unit flux accounts for the bed porosity n; i.e. if $\overline{q}_m$ is the mass per width and time at a point, the unit flux at that point is $\overline{q} = \overline{q}_m/\rho_s(1-n)$, where ρ_s is the density of the sediment. The sediment prism is characterized by its height $h(x,t)$ above the current sea level $z = \ell(t)$. At some time $t > 0$ (figure 1), the sediment prism consists of two parts: (i) the sediment, contained between the shoreline $x = s_2(t) > 0$ moving in the positive x-direction (always defined to be seaward), and the alluvial–bedrock transition $x = s_1(t) < 0$ moving in the negative x-direction (landward); (ii) a submarine sediment wedge deposited beyond the shoreline $x = s_2(t) > 0$. Following the arguments first made by Paola, Heller & Angevine (1992) and elaborated in the Appendix, we assume that the transport of the sediment over the sub-aerial fluvial surface is described by the diffusive flux

$$\overline{q} = -\nu \frac{\partial h}{\partial x}, \tag{2.1}$$

where the diffusivity ν is, in general, a function of the characteristic sediment grain diameter d and the time-averaged water unit discharge $\overline{q}_w$ over the fluvial surface (Swenson *et al.* 2000). In the Appendix we discuss the validity of a linear diffusion model and develop forms for ν applicable to field and experimental scenarios. In the submarine domain, we assume that the time and magnitude scales of slope evolution are small compared to those in the fluvial system. In this way, the slope of the foreset sediment wedge can be assumed to have a constant angle of repose α (Swenson *et al.* 2000; Voller *et al.* 2004). These transport behaviours can be incorporated into the Exner sediment balance equation (Paola & Voller 2005) to arrive at the following governing transport equation:

$$\frac{\partial h}{\partial t} = \nu \frac{\partial^2 h}{\partial x^2}, \quad s_1(t) \leqslant x \leqslant s_2(t). \tag{2.2}$$

The initial conditions are $\ell(0) = h(x,0) = 0$. The appropriate boundary conditions are

$$h|_{x=s_1(t)} = -\beta s_1(t), \tag{2.3a}$$

$$h|_{x=s_2(t)} = \ell(t), \tag{2.3b}$$

$$\nu \frac{\partial h}{\partial x}\bigg|_{x=s_1(t)} = -\overline{q}_0, \tag{2.3c}$$

$$\nu \frac{\partial h}{\partial x}\bigg|_{x=s_2(t)} = -\frac{\beta s_2 + \ell}{\alpha - \beta}\left(\alpha \frac{\mathrm{d}s_2}{\mathrm{d}t} + \frac{\mathrm{d}\ell}{\mathrm{d}t}\right). \tag{2.3d}$$

The first two conditions fix the sediment elevation to coincide with that of the bedrock basement at the alluvial–bedrock transition $x = s_1(t)$ (2.3*b*) and with the current sea level at the shoreline $x = s_2(t)$ (2.3*c*). The third condition (2.3*d*) sets the alluvial–bedrock transition to be the point at which the fluvial sediment flux matches the input flux; upstream of this transition the sediment is transported over the rock basement without either erosion or deposition. The last condition (2.3*d*),

https://doi.org/10.1017/S0022112009006715 Published online by Cambridge University Press

initially derived by Swenson *et al.* (2000), is essentially a statement of the mass balance at the shoreline; the flux of sediment arriving at the shoreline is balanced by the requirements of maintaining the geometry of the submarine sediment wedge, compensating for sea-level rise/fall and moving the shoreline forward.

3. The similarity solution

We develop a similarity solution of (2.2) and (2.3) under the condition that the sea level remains fixed at $\ell(t)=0$. The development of this solution essentially follows the approach previously used by Voller *et al.* (2004) and Capart and co-workers (Capart *et al.* 2007; Lai & Capart 2007). A key feature in this case, however, is that the resulting solution allows for the simultaneous existence of two moving boundaries, the shoreline $s_2(t)$ and the alluvial–bedrock transition $s_1(t)$; the previous solutions (e.g. Voller *et al.* 2004; Capart *et al.* 2007; Lai & Capart 2007) allow for only a single moving boundary. On setting the movement of the alluvial–bedrock transition (ab) and the shoreline (sh) to be respectively

$$s_1 = -2\lambda_{ab}(\nu t)^{1/2}, \tag{3.1a}$$

$$s_2 = 2\lambda_{sh}(\nu t)^{1/2}, \tag{3.1b}$$

introducing the similarity variable

$$\xi = \frac{x}{2(\nu t)^{1/2}} \tag{3.2}$$

and scaling the sediment height by

$$\eta = \frac{h}{2(\nu t)^{1/2}} \tag{3.3}$$

(2.2) and (2.3) reduce to the ordinary differential equation

$$\frac{1}{2}\frac{\mathrm{d}^2\eta}{\mathrm{d}\xi^2} + \xi\frac{\mathrm{d}\eta}{\mathrm{d}\xi} - \eta = 0, \quad -\lambda_{ab} \leqslant \xi \leqslant \lambda_{sh}, \tag{3.4}$$

with

$$\eta|_{\xi=-\lambda_{ab}} = \beta\lambda_{ab}, \tag{3.5a}$$

$$\eta|_{\xi=\lambda_{sh}} = 0, \tag{3.5b}$$

$$\nu\frac{\mathrm{d}\eta}{\mathrm{d}\xi}\bigg|_{\xi=-\lambda_{ab}} = -\overline{q}_0, \tag{3.5c}$$

$$\frac{\mathrm{d}\eta}{\mathrm{d}\xi}\bigg|_{\xi=\lambda_{sh}} = -2\gamma\lambda_{sh}^2. \tag{3.5d}$$

In (3.5d) the compound slope

$$\gamma = \frac{\alpha\beta}{\alpha-\beta} \tag{3.6}$$

is defined as the effective foreset slope; the product of this slope with the shoreline position $s_2(t)$ provides the water depth at the toe of the submarine sediments. The solution of (3.4), satisfying conditions (3.5b) and (3.5c), is

$$\eta(\xi) = \frac{\overline{q}_0}{\nu}\left(\lambda_{sh}\left(\frac{\mathrm{e}^{-\xi^2} + \pi^{\frac{1}{2}}\xi(\mathrm{erf}(\xi)+\mathrm{erf}(\lambda_{ab}))}{\mathrm{e}^{-\lambda_{sh}^2} + \pi^{\frac{1}{2}}\lambda_{sh}(\mathrm{erf}(\lambda_{ab})+\mathrm{erf}(\lambda_{sh}))}\right) - \xi\right), \tag{3.7}$$

https://doi.org/10.1017/S0022112009006715 Published online by Cambridge University Press

where $\mathrm{erf}(x) = (2/\sqrt{\pi}) \int_0^x \mathrm{e}^{-t^2} \mathrm{d}t$ is the error function. Using (3.7) in the remaining two boundary conditions, (3.5*a*) and (3.5*d*), we obtain nonlinear equations in the moving boundary constants λ_{ab} and λ_{sh} in (3.1):

$$\frac{R_{ab}\mathrm{e}^{-\lambda_{sh}^2}}{\mathrm{e}^{-\lambda_{sh}^2} + \pi^{\frac{1}{2}}\lambda_{sh}(\mathrm{erf}(\lambda_{ab}) + \mathrm{erf}(\lambda_{sh}))} = 2\lambda_{sh}^2 R_{sh}, \tag{3.8a}$$

$$\frac{R_{ab}\mathrm{e}^{-\lambda_{ab}^2}}{\mathrm{e}^{-\lambda_{sh}^2} + \pi^{\frac{1}{2}}\lambda_{sh}(\mathrm{erf}(\lambda_{ab}) + \mathrm{erf}(\lambda_{sh}))} = \frac{\lambda_{ab}}{\lambda_{sh}}(1 - R_{ab}), \tag{3.8b}$$

where the shoreline slope ratio $R_{sh} = \gamma/\beta = \alpha/\alpha - \beta$ is the ratio of the effective foreset slope (3.6) to the bedrock slope, and the alluvial–bedrock slope ratio $R_{ab} = \overline{q}_0/\nu\beta$ is the ratio of the fluvial to bedrock slopes at the alluvial–bedrock transition. Note that the physical nature of the problem constrains $R_{sh} \geqslant 1$ and $0 < R_{ab} < 1$. Solving the system (3.8) for λ_{sh} and λ_{ab} provides for simultaneous tracking of the shoreline $s_2(t) = 2\lambda_{sh}(\nu t)^{1/2}$ and the alluvial–bedrock transition $s_1(t) = -2\lambda_{ab}(\nu t)^{1/2}$ with time.

4. Limit solutions

In the limit $R_{ab} \to 1$, (3.8*b*) requires that the alluvial–bedrock transition be set at $x \to -\infty$, i.e. $\lambda_{ab} \to \infty$. Substituting this limit into (3.8*a*) generates the following equation for a finite value of λ_{sh}:

$$2\lambda_{sh}^2 \frac{\alpha}{\alpha - \beta} + \frac{\lambda_{sh}\pi^{\frac{1}{2}}(1 + \mathrm{erf}(\lambda_{sh}))}{\mathrm{e}^{-\lambda_{sh}^2} + \pi^{\frac{1}{2}}\lambda_{sh}(1 + \mathrm{erf}(\lambda_{sh}))} - 1 = 0. \tag{4.1}$$

This limit solution corresponds to fixing the alluvial–bedrock transition at $x = -\infty$ for all time $t \geqslant 0$ and tracking the movement of the shoreline into an ocean with a fixed level. A similarity solution specifically for this limit case has been previously developed by Capart *et al.* (2007), and we note that (4.1) corresponds to the fixed sea-level solution presented in this work: compare (4.1) with (57) in Capart *et al.* (2007). In the limit $R_{ab} \to 0$ there are two possible solutions. From (3.8) it is easy to see that a trivial solution of zero movement of the shoreline and alluvial–bedrock transition results for the cases in which $R_{ab} \to 0$ via $\overline{q}_0 \to 0$ (with ν and β fixed) or $\beta \to \infty$ (with ν and $\overline{q}_0$ fixed). The first condition corresponds to zero sediment delivery to the system and the second to the case of an infinitely deep ocean that removes all sediment supplied without forming a sediment prism. A non-trivial solution, however, exists when $R_{ab} \to 0$ via $\nu \to \infty$ (with β and $\overline{q}_0$ fixed). This limit does indeed set $\lambda_{ab} \to 0$ and $\lambda_{sh} \to 0$, but on multiplying both sides of (3.8) by ν it is noted that $(\lambda_{ab}\nu^{1/2}) \to 0$ and $(\lambda_{sh}\nu^{1/2}) \to \sqrt{\overline{q}_0/2\gamma}$. Hence, for this case, although the alluvial–bedrock transition is fixed at $x = 0$ for all time, the shoreline moves according to

$$s_2 = \sqrt{\frac{2\overline{q}_0 t}{\gamma}}. \tag{4.2}$$

The geometry of this problem simply involves a submarine sediment wedge with a horizontal fluvial surface coinciding with sea level and a foreset slope α prograding along the bedrock slope β. In this case, (4.2) can be readily derived from a simple mass balance. Indeed, the result in (4.2) matches the result obtained from the general geometric model of Kim & Muto (2007) under the assumption of a horizontal fluvial surface and no sea-level rise.

https://doi.org/10.1017/S0022112009006715 Published online by Cambridge University Press

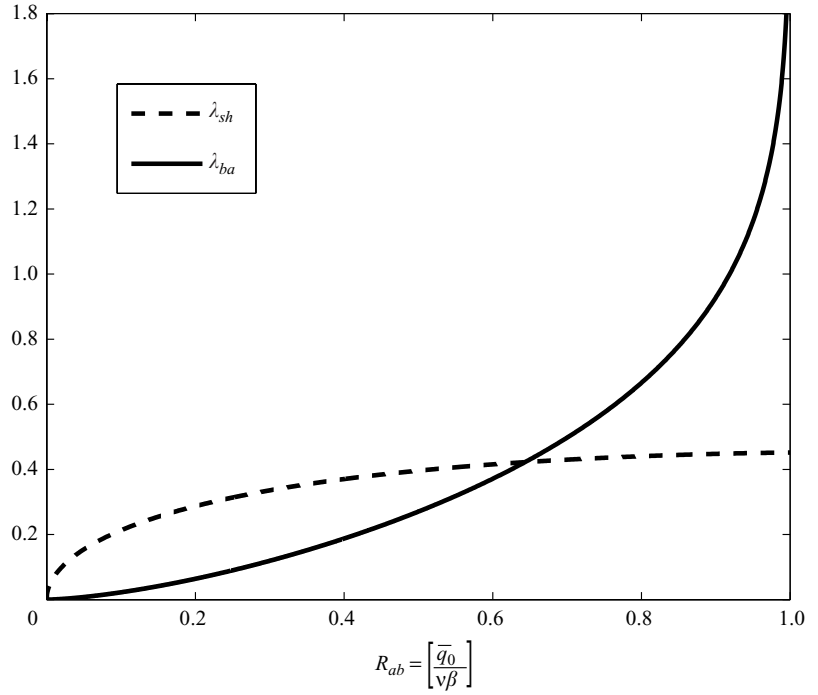


FIGURE 2. The solution space for the moving boundary parameters in (3.10) in the field-relevant case in which $R_{sh} = \gamma/\beta = 1$.

5. The solution space

For field conditions the foreset slope, α, is typically much greater than the bedrock slope, β, and the shoreline slope ratio $R_{sh} \approx 1$. Hence the physical solution space $(\lambda_{ab}, \lambda_{sh})$ can be characterized by plotting the solutions of (3.8) against $0 < R_{ab} < 1$ while keeping the shoreline slope ratio fixed at $R_{sh} = 1$. This plot is shown in figure 2. As a companion to this result the plots of the derivatives $\mathrm{d}\lambda_{ab}/\mathrm{d}R_{ab}$ and $\mathrm{d}\lambda_{sh}/\mathrm{d}R_{ab}$ are given in figure 3. The latter plot indicates the sensitivity of the moving boundary trajectories to changes in the value of the alluvial–bedrock slope ratio R_{ab}. As R_{ab} increases the movement of the alluvial–bedrock transition becomes increasingly sensitive to changes in R_{ab}, while the shoreline trajectory becomes less sensitive. For $R_{ab} < 0.2$ the movement of the shoreline is more sensitive than the movement of the alluvial–bedrock transition. The situation reverses above $R_{ab} \sim 0.2$: the alluvial–bedrock transition is more sensitive to changes in R_{ab} than the shoreline. The results in figures 2 and 3 have an important consequence for the interpretation of the stratigraphic record. With an appropriate definition of the diffusivity (e.g. Swenson *et al.* 2000) the alluvial–bedrock slope ratio can be written as a function of the characteristic sediment type (gravel or sand), the water unit discharge $\overline{q}_w$ and the sediment unit discharge $\overline{q}_0$, all key environmental parameters. Hence, in inferring past environmental changes in field sites at which the alluvial–bedrock slope ratios have $R_{ab} > 0.2$, the alluvial–bedrock transition is a more sensitive 'signal recorder' than the shoreline. The reverse is true if $R_{ab} < 0.2$. Both cases are possible in the field. We note, for example, that stratigraphic records in the Gulf of Mexico (Anderson & Fillon 2004) indicate alluvial–bedrock slope ratios in the range $0.2 < R_{ab} < 0.8$, while

https://doi.org/10.1017/S0022112009006715 Published online by Cambridge University Press

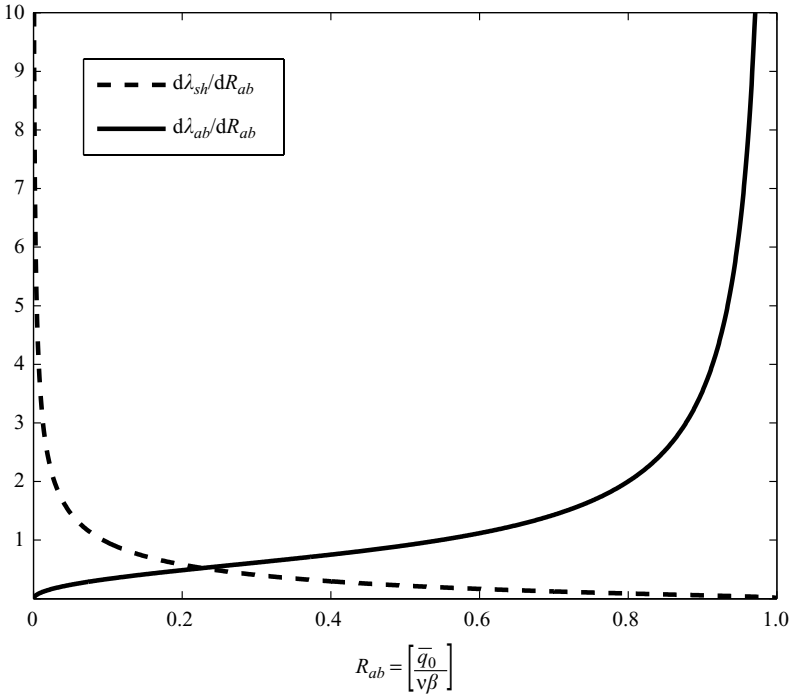


FIGURE 3. Sensitivity of the moving boundary trajectories to changes in the value of the alluvial–bedrock slope ratio R_{ab}.

basins bounded by steep normal faults (e.g. Crowell 2003) would have vanishingly small values of R_{ab}.

6. Comparison with experiment

We turn next to data from the experimental flume set-up at Nagasaki University, Japan, reported in Parker & Muto (2003), Muto & Swenson (2005, 2006), Kim & Muto (2007) and Swenson & Muto (2007), to provide experimental values to compare with the similarity solution given by (3.1) and (3.8). The experiments involved a narrow open-ended flume, 0.02 m wide, 4.3 m long and 1.3 m deep, immersed inside a larger tank (figure 4). Both tank and flume contained fresh water. A weir placed at the downstream end of flume, above the tank water level, ensured a constant water depth in the flume. Separate water and sediment (quartz sand with uniform 0.2 mm grain diameter and a density $\rho = 2598\,\mathrm{kg\ m^{-3}}$) fluxes were mixed in a funnel and delivered to the upstream end of the flume. The sediment was transported down the flume as bed load with a typical water depth of $\sim$1 mm. The inclination of the flume floor (the bedrock slope β), the unit sediment discharge $\overline{q}_0(\mathrm{mm^2\ s^{-1}})$ and unit water discharge $\overline{q}_w(\mathrm{mm^2\ s^{-1}})$ were varied to provide the nine sets of experimental conditions summarized in table 1. Since the channel width was much greater than the water depth the Reynolds number for the flow in the flume, upstream of the shoreline, could be calculated as $Re = \rho q_w/\mu$. From table 1 this gives Reynolds numbers in the range $189 < Re < 879$; appealing to open channel flow, this suggests that the flow in the experiments was in the laminar or transitional regimes. The flow velocities upstream of the shoreline ranged between 189 and 879 mm s^{-1}. There was rapid deceleration when the flow reached and moved downstream of the shoreline, leading

https://doi.org/10.1017/S0022112009006715 Published online by Cambridge University Press

	$\overline{q}_w$ (mm^2 s^{-1})	$\overline{q}_0$ (mm^2 s^{-1})	β
Run 1	878.65	42.80	0.1705
Run 2	733.10	42.80	0.1705
Run 3	579.10	42.80	0.1705
Run 4	562.25	42.80	0.2294
Run 5	335.45	42.80	0.2294
Run 6	232.15	42.80	0.2294
Run 7	229.95	13.46	0.1705
Run 8	220.45	13.46	0.2294
Run 9	188.75	42.80	0.2294

TABLE 1. Experimental set-up conditions.

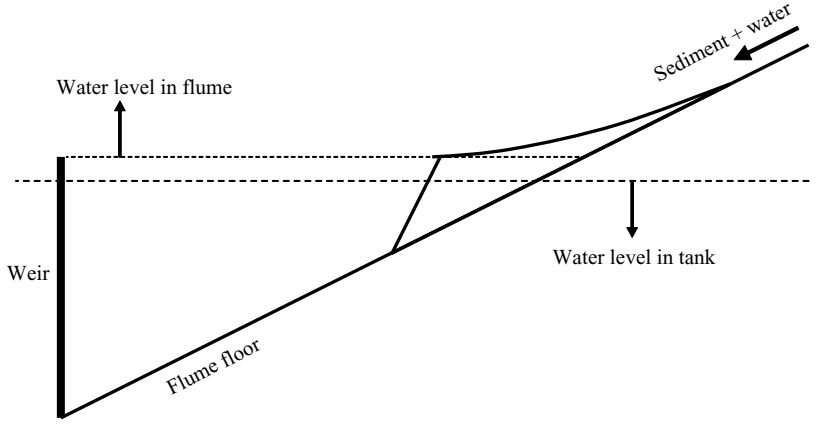


FIGURE 4. Schematic of experimental flume.

to sediment deposit on to the submarine wedge. As noted previously this sediment was redistributed by avalanche processes such that a wedge with a constant angle of repose was maintained. Beyond a few millimetres of the shoreline there was no notable disturbance of the water surface.

For each experimental condition, high-resolution photographs, taken every 20 s, detailed the evolution of the sediment prism. Digital analysis of these photographs provided a record of the positions, measured from the original shoreline at $x = 0$, of the alluvial–bedrock transition L_{ab}, the shoreline L_{sh} and the intersection of the foreset with the bedrock (the 'toe') L_{toe}. In order to obtain analytical predictions for the trajectories of the shoreline and alluvial–bedrock transition we need to know, for a given system, the input sediment flux $\overline{q}_0$, the bedrock slope β, the porosity of the deposit, the shoreline slope ratio $R_{sh} = \alpha/\alpha - \beta > 1$ and the alluvial–bedrock slope ratio $0 < R_{ab} = [\overline{q}_0/\nu\beta] < 1$. To make a valid comparison between analytical predictions and experiments these constant parameters have to be determined from measurements taken at a single time, which on subsequent use in the analytical solution recover the experimental measurements through time. The values of $\overline{q}_0$ and β are part of the experimental set-up conditions (see table 1). The porosity of the deposited sediment was assumed to be 0.3; this value was chosen by comparing an experimental final time image of the deposit area to the know sediment input. Since the foreset slope is assumed linear, $\alpha = \beta L_{toe}/L_{toe} - L_{sh}$, the shoreline slope ratio is

https://doi.org/10.1017/S0022112009006715 Published online by Cambridge University Press

readily determined as

$$R_{sh} = \frac{L_{toe}}{L_{sh}}. \tag{6.1}$$

The estimation of the alluvial–bedrock slope ratio, however, is a little more involved. First it is noted that for a small increment Δs in the shoreline movement the volume of sediment deposited offshore is given by $\Delta s L_{toe} \beta$. In contrast, on assuming that the curvature of the fluvial surface is large, the volume deposited on the fluvial surface can be approximated as $\Delta s L_{ab} \beta$. In this way, the sediment flux at the shoreline can be expressed as the following fraction of the input sediment flux:

$$\overline{q}_{sh} = \overline{q}_0 \frac{L_{toe}}{L_{toe} + L_{ab}}. \tag{6.2}$$

Further, we note that the average fluvial sediment flux on the fluvial surface (defined as the product of diffusivity and average slope) can be written as a weighted average of the input and shoreline fluxes, i.e.

$$\nu \frac{\beta L_{ab}}{L_{sh} + L_{ab}} = \phi \overline{q}_0 + (1 - \phi) \overline{q}_{sh}, \tag{6.3}$$

where $0 \leqslant \phi \leqslant 1$. On combining (6.2) with (6.3) and rearranging, we arrive at the following estimate for the alluvial–bedrock slope ratio in terms of the experimental measurement at a fixed point in time:

$$R_{ab} = \frac{\left(\frac{L_{ab}}{L_{sh}+L_{ab}} \right)}{\left(\phi + (1 - \phi) \frac{L_{toe}}{L_{toe}+L_{ab}} \right)}. \tag{6.4}$$

To be fully determined we need a choice for the weighting factor ϕ. The choice of $\phi = 1$ corresponds to assuming that the fluvial surface is linear, which contradicts the assumption of a diffusive flux that would build a concave surface. The choice of any other constant (e.g. $\phi = 0.5$) will, in the limit of $L_{ab} \to \infty$, result in non-physical values of $R_{ab} > 1$. Hence, a choice of weighting that varies between 0 and 1 in the physical limits of $0 < L_{ab} < \infty$ is needed. Here, based on assuming the weighting is a function of the fractions of the shoreline and alluvial–bedrock lengths, we use the choice

$$\phi = \frac{L_{ab}}{L_{sh} + L_{ab}}. \tag{6.5}$$

Table 2 reports the values of R_{sh} and R_{ab} obtained from the experimental measurements through (6.1), (6.4) and (6.5). These values, reported in terms of the mean μ_R and the standard deviation σ, are obtained by making estimations at each time step in the range $0.1 t_{end} < t < t_{end}$ (t_{end} is the total experimental run time); in all cases the sample size exceeded 100. From knowledge of the behaviour of the analytical solution it is known that predictions are relatively insensitive to changes in the value of R_{sh} but, especially at values close to 1, sensitive to changes in the alluvial–bedrock ratio R_{ab}. As such, in comparing the analytical predictions with the experimental measurements we use two realizations. While both use the mean value of R_{sh} from table 2, the values for the alluvial–bedrock ratio R_{ab} are set at $\mu_R \pm 2\sigma$.

The analytical predictions for the shoreline and alluvial–bedrock transition trajectories obtained with the values in tables 1 and 2 are compared with the experimental measurements in figures 5–7. For most of the runs, there is a close match

https://doi.org/10.1017/S0022112009006715 Published online by Cambridge University Press

	R_{ab}		R_{sh}	
	μ_R	σ	μ_R	σ
Run 1	0.6519	0.0109	0.6649	0.0321
Run 2	0.7232	0.0091	0.6621	0.0250
Run 3	0.8024	0.0085	0.6689	0.0407
Run 4	0.6560	0.0177	0.6765	0.0210
Run 5	0.8087	0.0066	0.6528	0.0132
Run 6	0.8729	0.0077	0.6531	0.0126
Run 7	0.8626	0.0079	0.6053	0.0251
Run 8	0.6644	0.0163	0.6404	0.0099
Run 9	0.9139	0.0036	0.6394	0.0174

TABLE 2. The mean and standard deviations of the alluvial–bedrock and shoreline slope ratios obtained from experimental measurements.

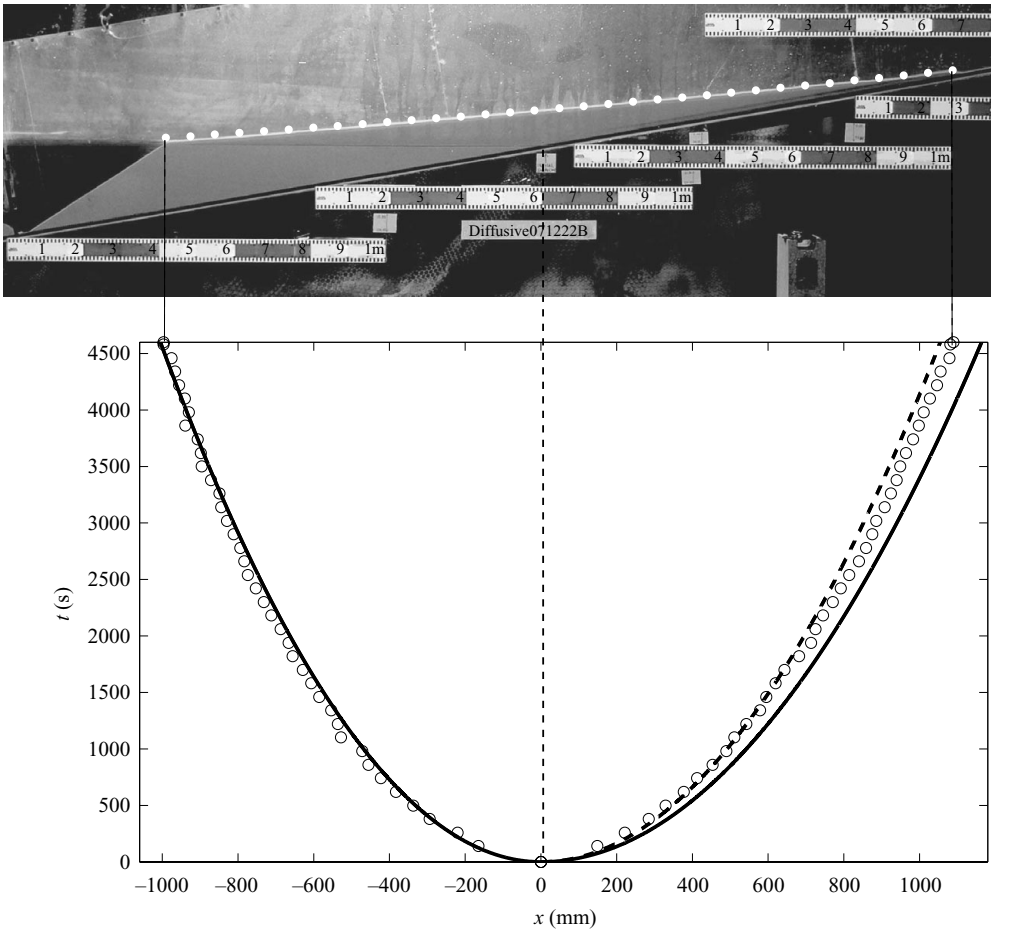


FIGURE 5. Experimental run 1. Predicted shoreline and alluvial–bedrock movements with time for $R_{ab} = \mu_R + 2\sigma$ (continuous line) and $R_{ab} = \mu_R - 2\sigma$ (dashed line) versus positions extracted from experimental images (open circles). The picture is the experimental image at time $t = t_{end}$. Superimposed on this image is the fluvial surface (white dots) given by the analytical solution when $R_{ab} = \mu_R$.

https://doi.org/10.1017/S0022112009006715 Published online by Cambridge University Press

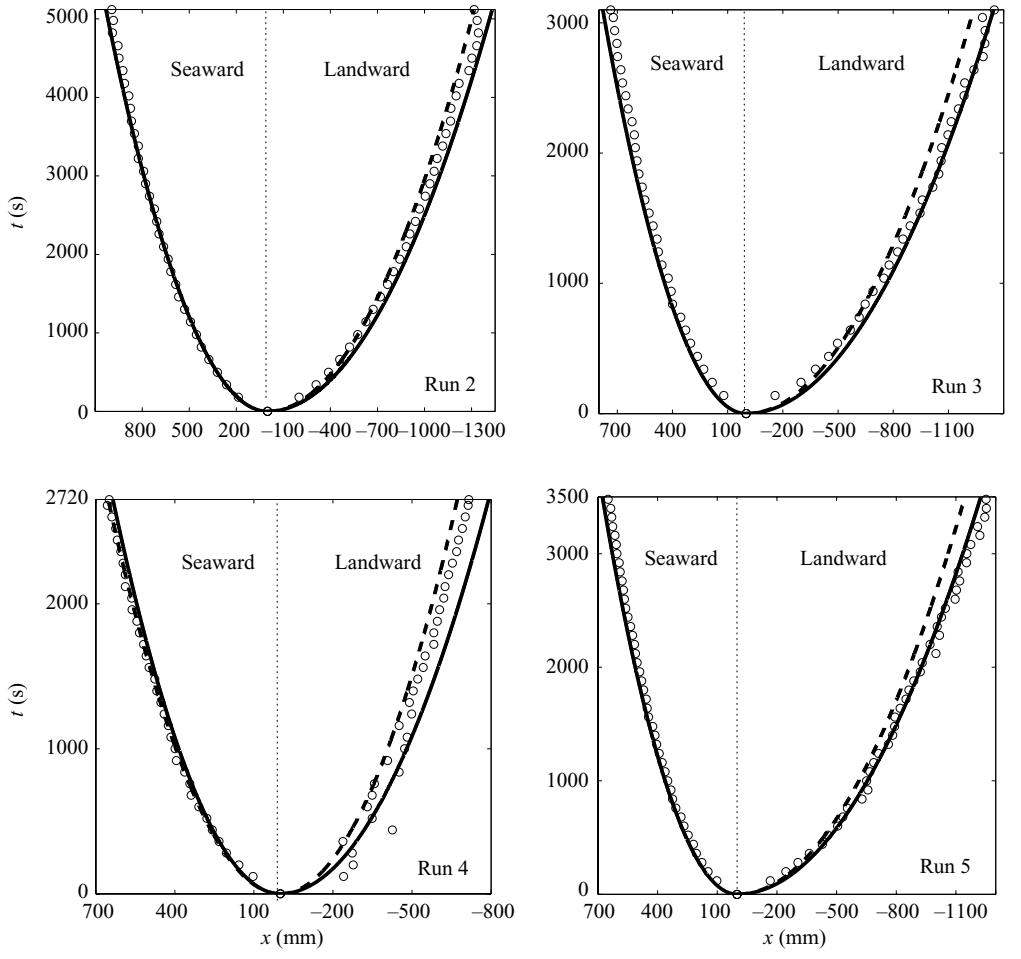


FIGURE 6. Experimental runs 2–5. Predicted shoreline and alluvial–bedrock movements with time for $R_{ab} = \mu_R + 2\sigma$ (continuous line) and $R_{ab} = \mu_R - 2\sigma$ (dashed line) versus positions extracted from experimental images (open circles).

between the analytical predictions and experimental measurements; in particular the upper and lower bound analytical predictions encompass the experimental measurements. In runs 6 and 9, however, there is a clear outward drift of the alluvial–bedrock transition measurements. This discrepancy can be attributed to the fact that these two runs correspond to the largest values of the alluvial–bedrock slope ratio R_{ab}, 0.8729 and 0.9139 (see table 2); from the above analysis we know when this ratio is close to unity, small changes in its value can have a significant effect on the movement of the alluvial–bedrock transition (see figure 3). This is verified on noting that with small increases in the estimated value of R_{ab}, obtained from (6.4), the analytical solution is able to predict alluvial–bedrock transition movement in close agreement with the measurement; e.g. figure 8 compares run 9 predictions when the estimated R_{ab} value is increased by 3 %.

In addition to the drifts noted above it may be observed that, at some instances, the measured movement of the alluvial–bedrock transition is erratic. This is attributed to the small angle of the sediment wedge at the alluvial–bedrock transition (see

https://doi.org/10.1017/S0022112009006715 Published online by Cambridge University Press

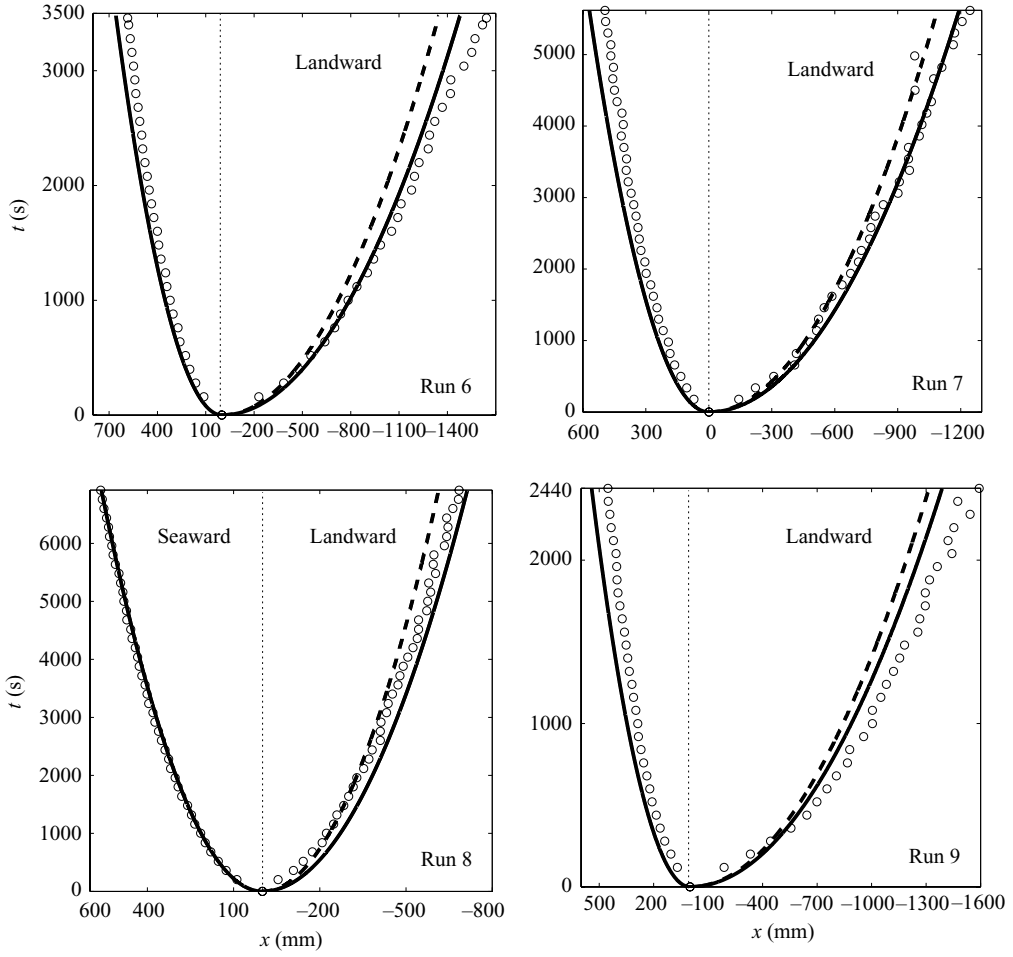


FIGURE 7. Experimental runs 6–9. Predicted shoreline and alluvial–bedrock movements with time for $R_{ab} = \mu_R + 2\sigma$ (continuous line) and $R_{ab} = \mu_R - 2\sigma$ (dashed line) versus positions extracted from experimental images (open circles).

photograph in figure 5). This feature makes the alluvial–bedrock transition region sensitive to local perturbations in sediment flux, leading to a loss in resolution of the exact position in the digital image.

Another factor that affects the comparisons between the solution and the experiment is the choice of porosity; the dependence of the moving boundaries on the porosity is given by $1/\sqrt{(1-n)}$. In particular, we note that an increase in porosity from the current value of $n = 0.3$ to $n = 0.4$ expands the envelope of the alluvial–bedrock transition and the shoreline in figures 5–7 by $\sim 7\,\%$.

7. A comment on sea-level rise

Under the assumption that sea level changes as the square root of time and is bounded from above by rate of the shoreline movement, an accounting of the sea-level variation can be readily incorporated in the closed-form similarity solution presented here. This prescription for sea-level rise, first used by Capart *et al.* (2007) in

https://doi.org/10.1017/S0022112009006715 Published online by Cambridge University Press

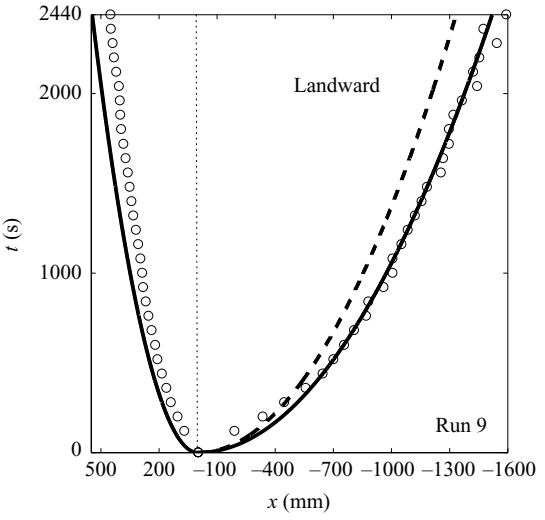


FIGURE 8. A large change in run 9 alluvial–bedrock transition predictions can be induced by a small increase in alluvial–bedrock slope ratio R_{ab}. Dashed line is the prediction of the alluvial–bedrock transition with original value $R_{ab} = 0.9139$ (table 2); solid line denotes the predictions with a 3 % increase ($R_{ab} = 0.9413$); and symbols signify experiments.

their single moving boundary model, does not however lead to any significant physical changes over the behaviour of the solution with a constant sea level. In particular, the common case of shoreline transgression during sea-level rise cannot be attained.

8. Conclusions

The main objective of this paper has been to study the solution to a moving boundary problem arising from the study of the long-term evolution of the coastal sedimentary prism. In keeping with previous work, this problem can be viewed as a generalized version of the well-known Stefan melting problem. The interesting feature here is the appearance of two moving boundaries, the alluvial–bedrock transition and the shoreline. The closed-form similarity solution for this dual moving boundary problem shows that the movement of the alluvial–bedrock transition becomes increasingly sensitive to environmental parameters (sediment type, sediment discharge and water discharge) as the ratio of the alluvial to bedrock slope increases. In particular, the analytical solution indicates that when the alluvial–bedrock slope ratio exceeds 0.2, a condition encountered in the field, determination of these parameters from preserved deposits is better done using the trajectory of the alluvial–bedrock transition than that of the shoreline, despite the emphasis on the latter in the earth-science literature.

The relatively simple nature of the problem studied has also allowed the use of experiments in a small laboratory flume to compare physical measurements with the analytical solution. Using estimation of solution parameters obtained from experimental measurements taken at single time, the analytical solution is able to recover the measured movements of the shoreline and alluvial–bedrock transition through time.

Clearly the problem studied here is also amenable to numerical solution, perhaps through using variations of the enthalpy method (Voller *et al.* 2006) or smooth particle

https://doi.org/10.1017/S0022112009006715 Published online by Cambridge University Press

hydrodynamics (SPH; Monaghan, Huppert & Worster 2005). While such solutions may not retain the precision or elegance of the analytical solution presented here, they will allow for the generation of solutions of more general problems, e.g. problem in multiple dimensions with arbitrary imposed changes in sea level.

Appendix. Argument for assuming a linear diffusion representation for the sediment flux

A key assumption in the diffusion model of sediment bed-load transport is that the line flux of sediment, q_s, at any location on the fluvial surface, is proportional to the local slope $S = \partial h/\partial x$ of the sediment–water interface, i.e. $q_s = -\nu \partial h/\partial x$, where ν is termed the 'fluvial diffusivity' (Paola *et al.* 1992). For completness, it is worthwhile to summarize the assumptions embodied in this relationship; Paola *et al.* (1992) provide a rigorous derivation of these 'diffusive' fluvial morphodynamics. We consider length scales $l > L_{bw}$, where $L_{bw} = h/S$ is the backwater length scale and h the average flow depth. In this case, the momentum balance reduces to the familiar depth-slope product, $\tau = ghS$, where τ is the kinematic bed shear stress (dimensions of $[L^2T^{-2}]$). Equivalently, the shear stress can be related to the average flow velocity U through a typical quadratic drag relationship, $\tau = C_f U^2$, where C_f is a friction coefficient. Combining these two relationships and allowing for the fact that in general only a fraction β $(0 < \beta \leqslant 1)$ of the fluvial surface is covered with flowing water, i.e. channelized, we arrive at

$$\tau^{3/2} = \beta^{-1} g q_w \sqrt{C_f} S, \tag{A 1}$$

where $q_w = Uh$ is the depth-integrated water flux. Note in a laboratory flume the water discharge q_w is a constant. A constant value for q_w can also be assumed for field settings, provided tributary input is minimal, a common feature in depositional systems.

In fully turbulent field settings, the friction coefficient C_f (A 1) is a weak (logarithmic) function of relative roughness and for present purposes can be taken to be approximately constant. In contrast, in small-scale laboratory flume settings the flow is often laminar to transitional, and so the friction coefficient is a function of the flow conditions. In particular, for a slot-like flume of constant width w, with a fully wetted surface ($\beta = 1$) and shallow flow depth $h \ll w$, the friction coefficient is a function of the grain diameter d and Reynolds number $Re = \rho q_w/\mu$, i.e. $C_f = f(Re, d)$.

There are two ways to progress from (A 1). First, consider a bed-load relation, such as the well-known Meyer-Peter & Muller (1948) formula, that can be written in the form

$$q_s^* = K(\tau_* - \tau_{*c})^{3/2}, \tag{A 2}$$

where $q_s^* = q_s/d\sqrt{g(s_g - 1)d}$ is dimensionless sediment flux; K is a constant (typically ~ 8); s_g is the specific gravity ($s_g = \rho_s/\rho \sim 2.65$); $\tau_* = \tau/g(s_g - 1)d$ is the dimensionless bed shear stress (the Shields number); and τ_{*c} is the dimensionless critical shear stress at which bed-load transport is initiated. Two limiting cases are of interest here. For bed-load-dominated rivers with weak banks, which in the field generally means gravel-bed rivers, the channel typically self-adjusts by widening to keep the bed shear stress slightly above critical, i.e. $\tau_* = (1 + \epsilon)\tau_{*c}$. The mechanistic justification for this is presented in Parker (1978), and further analysis and field evidence are presented in Parker *et al.* (2007). In this case (A 2) becomes $q_s^* = K((\epsilon/1 + \epsilon)\tau_*)^{3/2}$. Alternatively, as discussed in Dade & Friend (1998) and Parker *et al.* (1998), for most sand-bed and finer grained rivers the bed shear

https://doi.org/10.1017/S0022112009006715 Published online by Cambridge University Press

stress substantially exceeds the critical value, i.e. $\tau_* \gg \tau_{*c}$. In that case, (A 2) is modified to $q_s^* = K\tau_*^{3/2}$. Similarly, at the laboratory scale, where bed slopes are relatively large, e.g. $S \sim 0.1$–0.2, the bed shear stress is significantly larger than the critical shear stress. Consider, for example, the following representative values taken from the experiments reported in this work: sand particle diameter $d_s = 0.2$ mm, fluvial slope in the range $0.065 < S < 0.211$ and flow depth $h = 1.5$ mm. In this scenario the critical stress for motion is 7 to 21 times smaller than the stress applied on the bed surface (Ponce 1989, pp. 549–552). Hence in each of the above noted field and experimental settings the critical shear stress in (A 2) can be absorbed as a constant in the flux relationship or ignored altogether to arrive at, on combining (A 1) and (A 2), a linear relationship between the sediment flux and the local slope. More generally, we note that for any case in which a channel self-adjusts (e.g. via bank erosion) or is otherwise constrained to maintain a constant value of dimensionless shear stress τ_*, any sediment-flux relation of the form gives, with (A 2), a linear relationship between sediment flux and slope. For the specific scenarios above, the fluvial diffusivity ν has the form

$$\nu = \begin{cases} \dfrac{K\sqrt{C_f}}{\beta(s_g - 1)} q_w, & \text{field-scale, sand or finer,} \\ \dfrac{K\sqrt{C_f}}{\beta(s_g - 1)} \left(\dfrac{\epsilon}{1+\epsilon}\right)^{3/2} q_w, & \text{field-scale, gravel,} \\ \dfrac{K}{(s_g - 1)} (f(Re, d))^{1/2} q_w, & \text{slot–flume.} \end{cases}$$

Fluvial diffusivity is most sensitive to the water supply (q_w) in the system. Typically, q_w is assumed constant in field settings; i.e. tributary input is neglected; in experimental systems, q_w is a constant (upstream) input. The key point is that the sediment flux varies linearly with bed slope in both field- and laboratory-scale systems.

This work was supported by the STC program of the National Science Foundation via the National Center for Earth-surface Dynamics under the agreement number EAR-0120914. The authors would also like to thank Kyle Straub for discussions related to the values of the alluvial–bedrock slope ratio in the stratigraphy of the Gulf of Mexico.

REFERENCES

Anderson, J. B. & Fillon, R. H. (Ed.) 2004 *Late Quaternary Stratigraphic Evolution of the Northern Gulf of Mexico Margin*. Society for Sedimentary Geology.

Capart, H., Bellal, M. & Young, D. L. 2007 Self-similar evolution of semi-infinite alluvial channels with moving boundaries. *J. Sediment. Res.* **77**, 13–22.

Crank, J. 1984 *Free and Moving Boundary Problems*. Oxford University Press.

Crowell, J. C. (Ed.) 2003 *Evolution of Ridge Basin, Southern California: An Interplay of Sedimentation and Tectonics*. Geological Society of America.

Dade, W. B. & Friend, P. F. 1998 Grain size, sediment-transport regime and channel slope in alluvial rivers. *J. Geol.* **106**, 661–675.

Kim, W. & Muto, T. 2007 Two autogenic response of alluvial–bedrock transition to base-level variation: experiment and theory. *J. Geophys. Res.* **112**, F03S14. doi:10.1029/2006JF000561.

Lai, S. Y. J. & Capart, H. 2007 Two-diffusion description of hyperpycnal deltas. *J. Geophys. Res.* **112**, F03005. doi:10.1029/2006JF000617.

https://doi.org/10.1017/S0022112009006715 Published online by Cambridge University Press

Marr, J. G., Swenson, J. B., Paola, C. & Voller, V. R. 2000 A two-diffusion model of fluvial stratigraphy in closed depositional basins. *Basin Res.* **12**, 381–398.

Meyer-Peter, E. & Muller, R. 1948 Formulas for bed-load transport. In *Second Meeting of the Intl Association for Hydraulic Structures Research*, Stockholm, Sweden.

Monaghan, J. J., Huppert, H. E. & Worster, M. G. 2005 Solidification using smoothed particle hydrodynamics. *J. Comput. Phys.* **206**, 684–705.

Muto, T. & Swenson, J. B. 2005 Large-scale fluvial grade as a nonequilibrium state in linked depositional systems: Theory and experiment. *J. Geophys. Res.* **110**, F03002. doi:10.1029/2005JF000284.

Muto, T. & Swenson, J. B. 2006 Autogenic attainment of large-scale alluvial grade with steady sea-level fall: an analog tank–flume experiment. *Geology* **34**, 161–164.

Paola, H C., Heller, P. L. & Angevine, C. L. 1992 The large-scale dynamics of grain-size variation in alluvial basins. Part 1. Theory. *Basin Res.* **4**, 73–90.

Paola, C. & Voller, V. R. 2005 A generalized Exner equation for sediment mass balance. *J. Geophys. Res.* **110**, F04014. doi:10.1029/2004JF000274.

Parker, G. 1978 Self-formed straight rivers with equilibrium banks and mobile bed. Part 2. The gravel river. *J. Fluid Mech.* **89**, 127–146.

Parker, G. & Muto, T. 2003 one-dimensional numerical model of delta response to rising sea-level. In *Proceedings of the Third IAHR Symposium, River, Coastal and Estuarine Morphodynamics* (ed. A. Sánchez-Arcilla & A. Bateman), pp. 558–570, IAHR.

Parker, G., Paola, C., Whipple, K. X. & Mohrig, D. C. 1998 Alluvial fans formed by channelized fluvial and sheet flow. Part 1. Theory. *J. Hydraul. Engng* **124**, 985–995.

Parker, G., Wilcock, P. R, Paola, C., Dietrich, W. E. & Pitlick, J. 2007 Physical basis for quasi-universal relations describing bankfull hydraulic geometry of single-thread gravel bed rivers. *J. Geophys. Res.* **112**, F04005. doi:10.1029/2006JF000549.

Ponce, V. M. 1989 *Engineering Hydrology, Principles and Practices*. Prentice Hall.

Posamentier, H. W., Allen, H. W., James, D. P. & Tesson, M. 1992 Forced regressions in a sequence stratigraphic framework: concepts, examples, and sequence stratigraphic significance. *AAPG Bull.* **76**, 1687–1709.

Sommerfield, C. K., Ogston, A.S., Mullenbach, B. L., Drake, D.E., Alexander, C. R., Nittrouer, C. A., Borgeld, J. C., Wheatcroft, R. A. & Leithold, E. L. (Ed.) 2007 *Continental-Margin Sedimentation: Transport to Sequence Stratigraphy*. Blackwell.

Swenson, J. B. & Muto, T. 2007 Response of coastal plain rivers to falling relative sea-level: allogenic controls on the aggradational phase. *Sedimentology* **54**, 207–221.

Swenson, J. B., Voller, V. R., Paola, C., Parker, G. & Marr, J. G. 2000 Fluvio-deltaic sedimentation: a generalized stefan problem. *Eur. J. Appl. Math.* **11**, 433–452.

Voller, V. R. 1997 A similarity for the solidification of multicomponent alloys. *J. Heat Mass Transfer* **40**, 2869–2877.

Voller, V. R., Swenson, J. B., Kim, W. & Paola, C. 2006 An enthalpy method for moving boundary problems on the earths surface. *Intl J. Heat and Fluid Flow* **16**, 641–654.

Voller, V. R., Swenson, J. B. & Paola, C. 2004 An analytical solution for a Stefan problem with variable latent heat. *Intl J. Heat Mass Transfer* **47**, 5387–5390.

Worster, M. G. 1986 Solidification of an alloy from a cooled boundary. *J. Fluid Mech.* **167**, 481–501.

https://doi.org/10.1017/S0022112009006715 Published online by Cambridge University Press